Environmental Interactions in the GFDL Hurricane Model for Hurricane Opal

JOHN PERSING, MICHAEL T. MONTGOMERY, AND ROBERT E. TULEYA*

Department of Atmospheric Science, Colorado State University, Fort Collins, Colorado

(Manuscript received 11 May 2000, in final form 30 July 2001)

ABSTRACT

Hurricane Opal (1995) crossed the Gulf of Mexico rapidly intensifying to a 130-kt storm, then fortunately weakening before landfall on the Florida panhandle. This intensification was underforecast by the National Hurricane Center. Forecast fields from the 1997 version of the Geophysical Fluid Dynamics Laboratory Hurricane Prediction System (GFDL model) for Hurricane Opal are used to diagnose the rapid intensification of the tropical cyclone. While falling short of the realized peak intensity, the simulation did capture the phase of intensification. This study presents the first step toward diagnosing the mechanisms for intensification within a moderate resolution (~15 km) hydrostatic model and testing the extant hypotheses in the literature.

Using a mean tangential wind budget, and the Eliassen balanced vortex model, positive eddy vorticity fluxes aloft are identified in the vicinity (~600 km) of Opal, but are not found to aid intensification. A detailed examination of each of the terms of the budget (mean and eddy vorticity flux, mean and eddy vertical advection, and ''friction'') shows for the most rapidly intensifying episodes a greater forcing for mean tangential winds near the center of the storm, particularly from the mean vertical advection and mean vorticity flux terms. Variations in these mean terms can be primarily attributed to variations in the heating rate. Upper-level divergence exhibits significant vertical structure, such that single-level or layer-average analysis techniques do not capture the divergence signature aloft. Far from the storm (≥400 km), divergence features near 200 mb are significantly influenced by convective events over land that are, perhaps, only indirectly influenced by the hurricane.

While there is a trough interaction simulated within the model, we suggest that the hurricane develops strongly without an important interaction with the trough. A synthetic removal of specific potential vorticity features attributed to the trough is proposed to test this hypothesis. Imposed shear is proposed to weaken the storm at later times, which is at odds with other recent ''nontrough'' theories for the behavior of Opal.

1. Introduction

Until recently, improvements in hurricane forecasting have focused primarily on track. The obvious benefit of an accurate track forecast is the selection of proper risk areas for emergency response, and this has been the main emphasis in improving hurricane forecasts in previous decades. Hurricane intensity forecasting, in contrast, has not improved to the same degree as track (DeMaria and Kaplan 1999). Better intensity forecasting has been identified as a target to improve forecasts of damaging winds of landfalling tropical cyclones (Marks et al. 1998). This paper presents the first opportunity to study the mechanisms for intensification within a hydrostatic model of moderate resolution (~15 km) and compare the results to an observed storm.

The heart of the hurricane intensity forecasting problem is the interaction of an intensely rotating, convecting vortex on the mesoscale (~50 km) with external influences such as winds, moisture, temperature, and surface heterogeneities (including land–sea differences) that affect the storm from the mesoscale to the synoptic scale (~1000 km). This represents a computational challenge that is gradually falling to improvements in computer technology. This paper will demonstrate how output from the Geophysical Fluid Dynamics Laboratory (GFDL) Hurricane Prediction System model (hereafter, GFDL model; Kurihara et al. 1995, 1998) was integrated into an analysis package for the purpose of identifying the important flow features evident in a simulation of Hurricane Opal (1995). The model provides an opportunity to study the interaction of an intensely rotating, convecting vortex in a reality-based, numerical representation of a broad, synoptic-scale troposphere. This study falls between the broad-scale examination of Molinari and Vollaro (1989, 1990) and the study of the internal responses of a hurricane in higher-resolution models (Liu et al. 1997, 1999; Zhang et al. 2000; Braun and Tao 2000). While a hurricane cannot yet be thoroughly observed at the mesoscale to provide an accurate initial representation of Opal, the evolution of the in-

* Current affiliation: NOAA/Geophysical Fluid Dynamics Laboratory, Princeton, New Jersey.

Corresponding author address: Dr. John Persing, Dept. of Atmospheric Science, Colorado State University, Fort Collins, CO 80523-1371.
E-mail: john@charney.atmos.colostate.edu

tensity of the vortex in the model mimicks well the intensity trend observed in Opal. Thus we believe the GFDL model is well positioned to model the response of a hurricane-like vortex to the observed, large-scale effects that are represented in the initialization. This dataset recently has been further applied by Möller and Shapiro (2001, manuscript submitted to *Mon. Wea. Rev.*, hearafter, MS) to analyze the internal structure of Opal.

The importance of environmental effects is evident in the monotonic, empirical relationship between the apparent maximum potential intensity (DeMaria and Kaplan 1994a; Bosart et al. 2000) and the skill that can be added to empirical forecasts by adding environmental variables (DeMaria and Kaplan 1999). Even within the maximum intensity framework, the instantaneous intensity of the cyclone is uniformly distributed between some minimum and an empirical maximum intensity (DeMaria and Kaplan 1994a; Emanuel 2000). This suggests that it is important to understand the life cycle of tropical cyclones and the influences that uniformly distribute storm intensity between those limits. Emanuel (1998) posited the role of vertical wind shear, turbulent mixing of cold water, a poor estimation of bulk aerodynamical constants, sea spray, and ocean bubbles to explain this distribution of intensity.

Molinari et al. (1998) argued that a superposition of an upper-level potential vorticity (PV) anomaly of small horizontal scale over the center of a nascent tropical cyclone spurred the initial intensification in Tropical Storm Danny (1985). Molinari and Vollaro (1990) diagnosed the approach of eddy angular momentum flux towards the center of Hurricane Elena (1985) and used Eliassen's (1952) balanced vortex model to show how such eddy fluxes can place the upper troposphere out of balance and induce a preference for ascent near the center of the developing hurricane. Wu and Cheng (1999) suggested the importance of eddy angular momentum fluxes, but showed in their examination of Typhoons Flo (1990) and Gene (1990) in the western Pacific that the upper-level PV features did not get close enough to the storm to promote a strong superposition interaction.

In this paper, we extend these approaches based on large-scale operational analysis fields by examining the environmental impact on storm intensity at moderate resolution. Motivated by the observational analysis of Bosart and Bartlo (1991), Montgomery and Farrell (1993) showed how an interaction with an upper-level trough of a type often associated with subtropical situations can lead to the genesis of tropical storms by acting upon a column of air with an approximately moist neutral profile. Using a dataset enhanced with satellite-derived winds, the recent work of Bosart et al. (2000; hereafter, B00) has shown the occurrence of divergence aloft associated with a jet entrance region coinciding with rapid intensification episodes in Hurricane Opal. Also noted in B00 was the influence of a warm ocean eddy in the Gulf of Mexico in the intensification of Hurricane Opal. It was found in B00 that the eddy flux convergences aloft are too far away to explain the axisymmetric outflow aloft. By correlating observed divergence with episodes of deep convection (inferred from satellite imagery), B00 suggested that the divergence aloft (attributed to the jet entrance region) spurred mesoscale convective events in the vicinity of Opal, which then led to intensification of the storm, perhaps augmented by either a vorticity redistribution process (Montgomery and Kallenbach 1997; Montgomery and Enagonio 1998) or through exchanges of angular momentum modified by convection (Krishnamurti et al. 1998).

Within the context of the GFDL model, these theories will be pitted against more traditional theories for hurricane intensification that operate on spatially uniform inputs such as benign vertical shear (Gray 1968). The recent work of Emanuel (1999) suggested that for many cases (including Opal, but not for all cases examined) an accurate hurricane intensity forecast can be performed by an axisymmetric model evolved from an initial vortex strength. The forecasts relied on knowledge of the sea surface temperature at the center of the storm, taking due account that complicating factors like hostile wind shear and ''wet swamps'' can lead to error in the formulation. But even within such a ''uniform'' environmental context, an explanation is desired for the rapid intensification of Hurricane Opal within the GFDL model.

This paper will focus on the applicability of GFDL operational model output fields for the diagnosis of hurricane intensity changes. Section 2 presents a brief description of the model and data processing. Section 3 summarizes features noted in the model simulation and relates these to theories of rapid hurricane intensification. A discussion follows in section 4 along with a proposed strategy for future research. The conclusions of this paper are summarized in section 5.

2. GFDL model overview and data procedure

a. GFDL model

Opal reached hurricane intensity off the northwest coast of the Yucatan Peninsula in the southern Gulf of Mexico at 1200 UTC 2 October 1995, according to the ''best track'' summary produced by the U.S. National Hurricane Center (NHC). After drifting slowly westward over the next 24 h, Opal began to traverse the Gulf of Mexico moving north-by-northeast around 1200 UTC 3 October 1995, intensifying from 80 to 130 kt by 1200 UTC 4 October 1995, then weakening prior to landfall on the Florida panhandle (Fig. 1, heavy, solid line).

For this study, the GFDL model was initialized at 1200 UTC 3 October 1995 and output was extracted at a 3-h interval until 36 h (0000 UTC 5 Oct 1995). Forecasts from the 1997 version of the model, more fully described by Kurihara et al. (1998), are used here. The

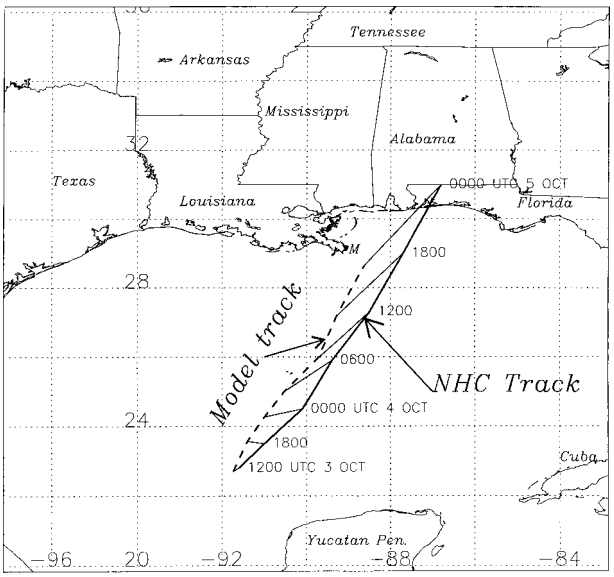

FIG. 1. The ''best track'' (heavy, solid) of Hurricane Opal and model forecast track (dashed). Thin solid lines connect model forecasts and verifications at each time and are a measure of error. The M near 29°N, 89°W denotes the mouth of the Mississippi River.

TABLE 1. GFDL Model σ levels for integration and p levels used in this analysis.

σ level	p level (mb)
0.9950	1000
0.9815	988
0.9605	967
0.9204	925
0.8563	860
0.7772	780
0.6881	690
0.5935	600
0.4974	500
0.4248	425
0.3748	375
0.3248	325
0.2747	275
0.2234	225
0.1746	175
0.1244	125
0.0740	75
0.0207	20

model is integrated in a terrain-following sigma coordinate system comprised of 18 vertical levels with dense coverage at lower levels (Table 1). Grid points are spaced within three interacting, grid domains: 1) a fixed, coarse (75° × 75°) domain of 1° grid spacing covering North America and the adjacent Pacific and Atlantic Oceans, and 2) two movable, finer-mesh domains of ⅓° and ⅙° grid spacing that are centered on the moving hurricane. The model output used here is simply the data fields from all three meshes interpolated to an intermediate grid mesh of ⅓° for the entire 75° × 75° fixed domain. This is a compromise dataset to allow output from the model over a complete forecast domain covering all of North America and the adjacent waters (examined, but not shown here) while still minimizing disk and computer costs during analysis. Spatiotemporal consistency of the vertical motion field as analyzed gives credence to our analysis of the coarse convective response shown later. Our focus here is on the large-scale forcings, which are well resolved at 30 km. The National Centers for Environmental Prediction (NCEP) analysis provides the initialization fields for the GFDL model, whereupon the vortex in those fields is filtered out and a new vortex is introduced based upon the observed location and intensity of the tropical storm. The new storm is introduced by a controlled spinup process (Kurihara et al. 1993, 1995, 1998). This version of the GFDL model has a fixed surface temperature and does not model any ocean interactions (for an example of a coupled GFDL–ocean simulation, see Bender and Ginis 2000).

The simulation of Opal is initialized at 1200 UTC 3 October 1995 beginning with an initial minimum surface pressure of 951 mb, then deepening to 917 mb over 24 h (Fig. 2). After 24 h, the central surface pressure weakens only slightly, until after 36 h (not shown) when the storm weakens considerably after landfall. The initialization routine ''fits'' the observed wind structure. Given the approximation due to the grid spacing, a deeper initial central pressure is needed to fit the observed winds. The surface pressure trace presented here is based on a diagnostic report from the model at a 1-h interval, not the 3-h interval full-data fields presented later. Comparison with an even higher temporal resolution pressure trace contained within the report (not

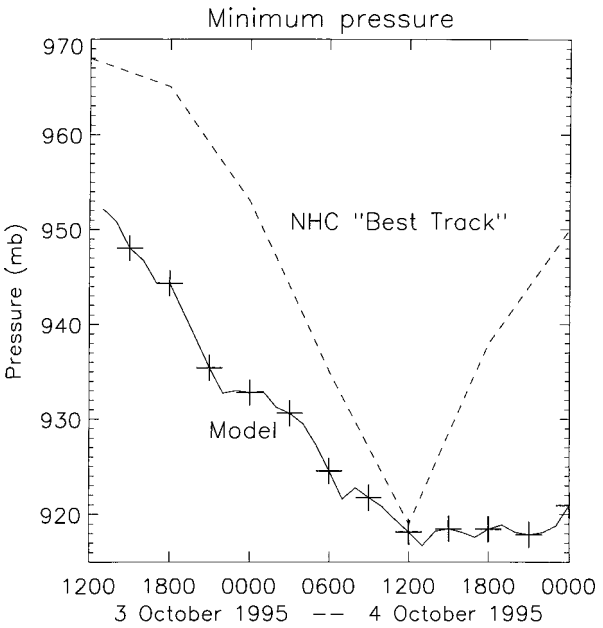

FIG. 2. Minimum simulated storm pressure (mb; solid) and that from the NHC best track (dotted). The crosses denote times where complete data fields are analyzed for this paper.

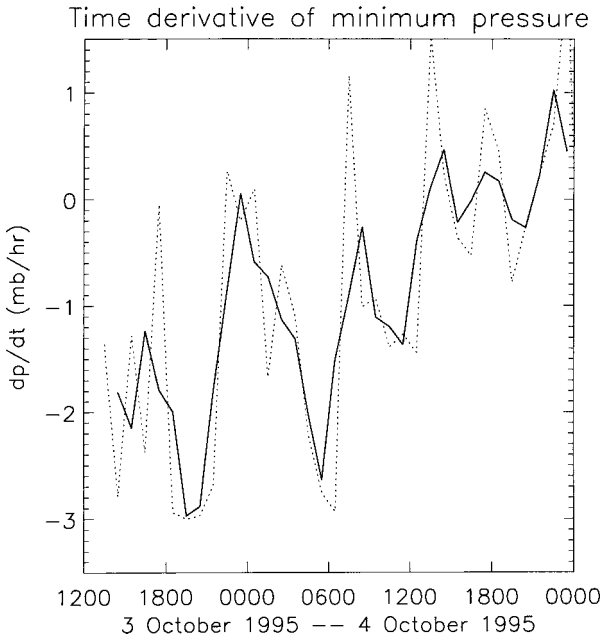

FIG. 3. Time rate of change of minimum pressure (mb h^{-1}) computed from the sample of pressures at 1-h intervals (dotted) and a 3-h running average of the same (solid).

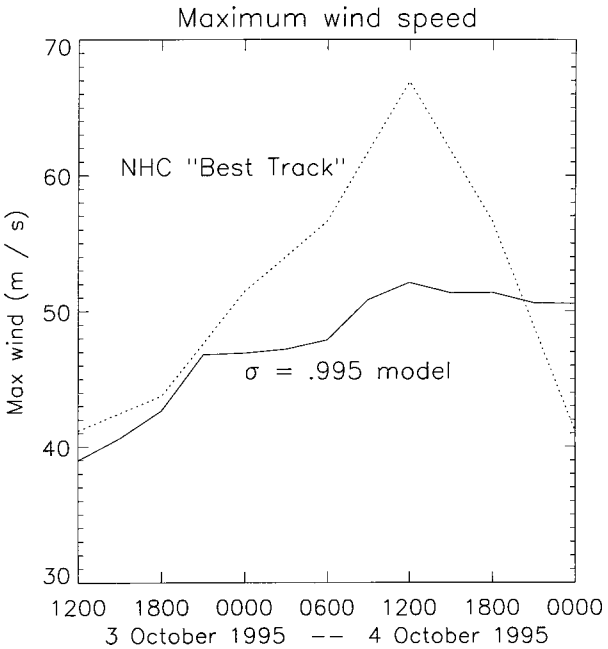

FIG. 4. Maximum wind speeds simulated in the lowest model level (solid) and that from the NHC best track (dotted).

shown) verifies that this 1-h pressure dataset tracks the important changes in intensity in the storm. The time rate of change of central pressure (Fig. 3) will be used to identify intensifying stages in the storm. The peak winds at the lowest model level (~50 m) are used for comparison with the observed maximum winds at 10 m (Fig. 4) in light of recent dropsonde observations (Franklin et al. 2000; Black and Franklin 2000).[1] As expected, the initialization procedure provides for an accurate initial wind, but the model is less responsive than the observed storm, reaching a 51 m s^{-1} maximum. The strongest winds observed in the free atmosphere reach 79 m s^{-1}. The magnitude of variations in peak winds and central pressure are not as pronounced as in the observed storm, but on the basis of these results it is concluded that the phase of intensification for Opal is captured by this simulation. In particular, two instances of rapid intensification beginning at 1800 UTC 3 October and 0400 UTC 4 October are interesting in light of two such instances found by B00 at 0000 UTC and 1000 UTC 4 October 1995.

Two possible explanations for the intensification before (and weakening after) 1200 UTC 4 October (B00) are modifications of the maximum potential intensity (MPI) determined from large-scale thermodynamic parameters and the passage of the eyewall over a warm core ocean eddy (WCE). The current simulation is not able to address the latter theory since sea surface temperatures (SSTs) are invariant in time and do not resolve any signature resulting from the WCE. There is a systematic bias in this version of the GFDL model to fill central surface pressures of hurricanes slowly during the decaying stage, possibly as a result of an unmodeled ocean interaction (Bender and Ginis 2000). The model hurricane tracks ~100 km to the west of the observed storm, making landfall at the mouth of the Mississippi River in Louisiana (Fig. 1). The track errors do not greatly affect the underlying environment because the storm remains over the ocean for the same amount of time as observed and the ocean has no spatial variations in thermal content. Noting this, track errors of the storm relative to the unresolved WCE are not important. Errors of this size, though much smaller than the scale of the upper-level trough, could impact whether the trough is beneficial to intensification (Molinari et al. 1998), but the guarded success of the intensity of the model storm might suggest that the trough interaction in this simulation is representative.

b. Data processing

To reduce the size of the dataset to a level where the relevant variables could be considered simultaneously through a graphical user interface, a minimal dataset was created by interpolating the rectilinear GFDL model data to a storm-centered, cylindrical coordinate system. The storm center is located to the nearest tenth of a grid square (~$\frac{1}{30}$°) at each time step using the minimum of the surface pressure field. A cylindrical grid is then

[1] Recent improvements in modeling the boundary layer in the GFDL model (subsequent to the present study) improve the wind–pressure relationship and better match the vertical structure noted in dropsonde observations.

defined with an outer radius of ~1000 km, a radial grid spacing approximating the original grid spacing (~⅓° or 33 km), and 60 azimuthal grid points. The grid points in the rectilinear grid are unequally spaced in real space due to spherical geometry. A simple linear correction is applied in projecting the grid points to x and y coordinates centered on the storm that accounts for more than 90% of the position error of grid points considering the limited domain and the low latitudes in question. A full consideration of the spherical geometry would be needed for a much larger analysis grid or at much higher latitudes. A bicubic interpolator is used for horizontal interpolations from rectilinear to cylindrical coordinates. In the present analysis, the vertical coordinate of the cylindrical grid is pressure, with vertical levels (Table 1) selected to approximate the original vertical resolution in sigma coordinates. The data fields are linearly interpolated in the vertical from sigma to pressure coordinates and a mask is identified where grid points fall below the ground or above the top sigma level.

3. An illustration of hurricane–trough interaction

Figure 5 illustrates a single absolute vertical vorticity isosurface at three times.[2] Colors are used for different vertical layers. The hurricane is evident as a nearly vertical tower of relative vorticity at the center of the analysis domain (the apparent offset is an aspect of the projection and low surface pressures at the center). A complex of stationary vorticity blobs (Fig. 5a) associated with the mountains of Mexico disappears from the foreground (Figs. 5b,c) as the analysis domain translates with the hurricane to the north-northeast. As the trough (and its cyclonically curved winds and vorticity) and the center of the hurricane approach one another, an increase of positive vorticity signature is evident to the north and west of the domain as time goes on (most evident in Fig. 5c). Midlevel vorticity at around 400 km from the center of the storm becomes more prevalent to the north and west of the storm and acquires a more filamented character with time (Figs. 5b,c). Low-level vorticity (in red) is organized in bands and shifts from an early preference south and east of the storm (Fig. 5a) to the north and west (Figs. 5b,c) and are generally located below regions of upward vertical motion (Figs. 16b,c compared with Figs. 5b,c).

The environmental flow is obviously affected by the presence of the storm. The presence of the trough northwest of the storm (Fig. 5c) is believed to influence the storm in several ways. First, it imposes an increased vertical shear across the storm. Second, it potentially provides an enhancement of the upper-level circulation of the storm through fluxes of eddy angular momentum (to be defined precisely later). These potential influences will be evaluated in turn.

a. Shear

Following the technique of Bender (1997), an environmental wind can be defined by averaging the model winds in an annulus between radii of 75 and 250 km on each pressure level. A measure of shear can then be defined by subtracting this environmental wind between two levels. The 850–200-mb shear defined in this manner is shown in Fig. 6. This measure follows closely other full-tropospheric measures of shear, for example, within a 600-km averaging radius found in DeMaria and Kaplan (1994b) and a 500-km averaging radius from B00.[3] Figure 7 shows the variation of 850–200-mb shear measures to variations in outer radius for the special case of having the inner radius of the annulus vanish (i.e., a filled circle). As can be seen, all averaging circles having a radius of more than 150 km (large enough so that asymmetric ''core'' effects near the storm contribute little to the sample) capture approximately the same signal, although the signal is most accentuated for radii between 200 and 400 km. Defining an annulus by using a nonzero inner radius (not shown) excludes the core and alters the computation only slightly.

Titley and Elsberry (1999) proposed that the cyclogenesis of Typhoon Flo (western Pacific, 1990) was related to a vertical extension of convection and cyclonic circulation to the tropopause, diagnosing this hypothesis by examining the wind profile across the tropopause. They noted an extension of lowered environmental wind speed through a greater depth of the atmosphere and suggested that the lowered shear across the 300–150-mb layer would be reflective of the presence of convective towers to this higher height. An application of this idea to the Opal dataset is presented in Fig. 6 with the dashed line. This measure is not strongly predictive (on an hour-by-hour basis) of either the storm intensity or intensification rate (Fig. 3), yet the weak overall signal can be seen as representing a favorable environment for intensification, with the increase in this measure at later times being a possible signal for limiting the intensification of Opal.

Interpretation of this result is complicated in the model simulation by sharp vertical shears in the environmental wind found in narrow vertical layers.[4] This suggests that the determination of shear will be sensitive to the selection of analysis layers. One test is presented in Fig. 8 where the upper analysis level is varied from

[2] Potential vorticity, while exhibiting many of the same features as vertical vorticity in the mid to lower troposphere, is more difficult to display because it exhibits high values in the stratosphere which would sit in the foreground and obscure tropospheric features.

[3] Following present operational practice at forecast offices and for comparison with the cited papers, vertical shear is expressed in terms of m s^{-1} as the magnitude of the vector difference between two pressure levels. A proper shear measure would divide through by an approximate depth between the two levels, about 10 km.

[4] The tropopause is generally found in the model at 125 mb, if the tropopause is defined as the point of rapid increase in vertical gradient of potential temperature.

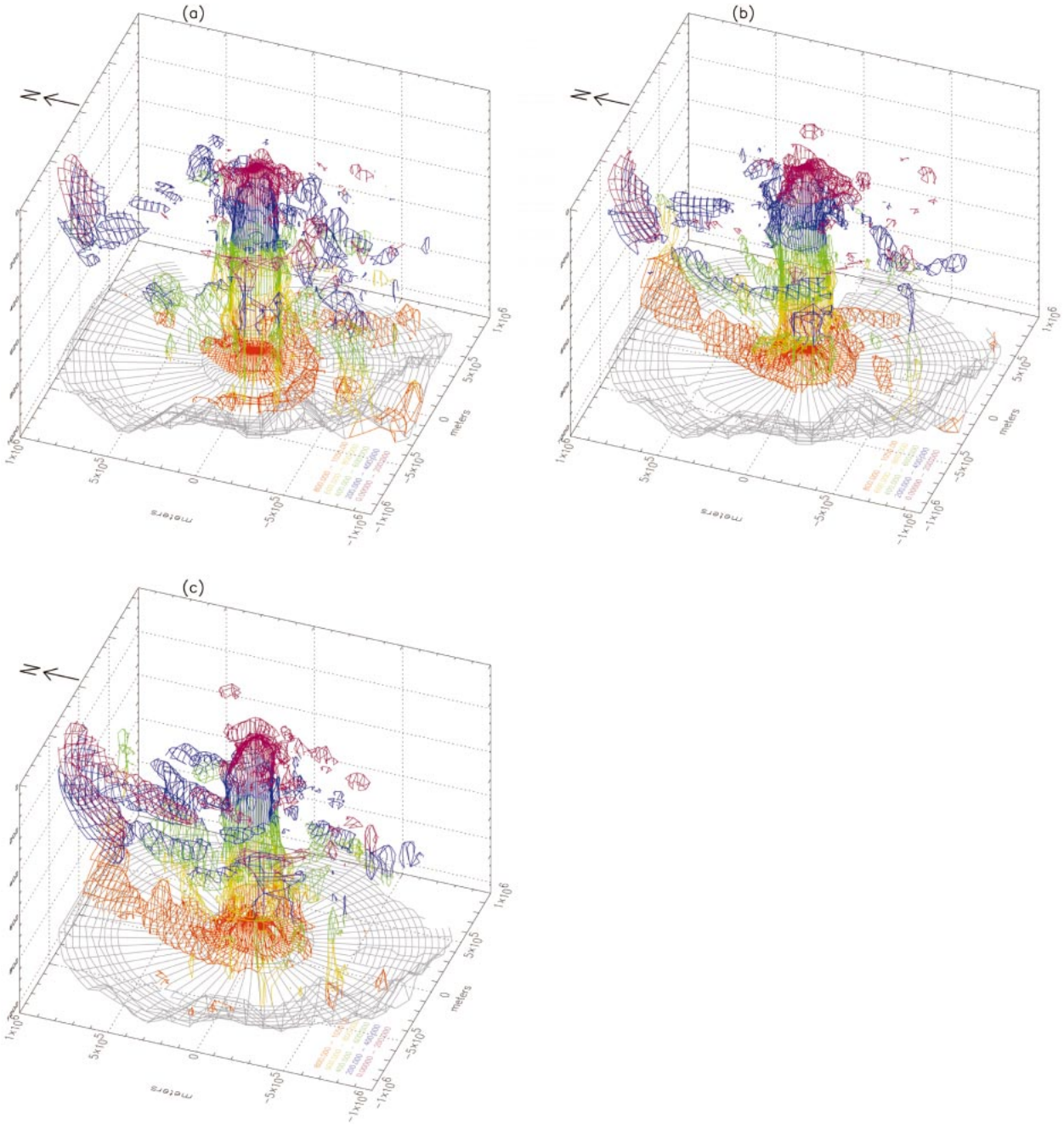

FIG. 5. The 1.15×10^{-4} s^{-1} isosurface of absolute vertical vorticity at (a) 2100 UTC 3 Oct, (b) 0300 UTC 4 Oct, and (c) 0900 UTC 4 Oct 1995. Colors denote vertical layers: Red = 1000–800 mb, yellow = 800–600 mb, green = 600–400 mb, blue = 400–200 mb, purple = above 200 mb. Gray represents the ground. Distances are in meters.

250 to 150 mb. Use of a lower analysis level captures an early modulation near the 250-mb level in upper-level winds, but use of the 150-mb level is sensitive (with a lag and with less magnitude) only to the later onset of shear. The environmental wind on each pressure level is presented in Fig. 9, which most closely resembles Bender's Fig. 12 (Bender 1997) for a simulation of a storm sheared from the rear. The component of storm-relative environmental wind in the direction of storm motion (Fig. 9a) gradually changes from front-to-rear at the surface to rear-to-front peaking around 250 mb, above which the imposed wind rapidly switches to front-to-rear again. The component of environmental wind perpendicular to storm motion (Fig. 9b) strengthens to

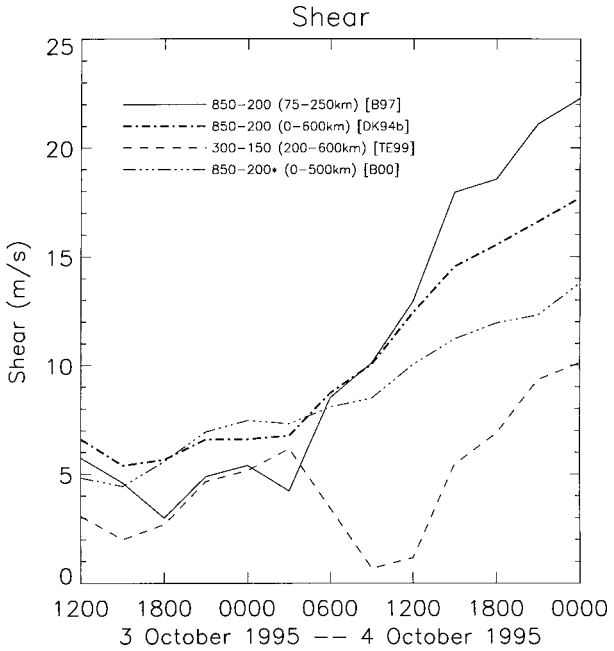

FIG. 6. Vertical wind shear measures. The solid line is based on Bender (1997), the dash–dotted line on DeMaria and Kaplan (1994b), the dashed line on Titley and Elsberry (1999), and the dash–triple-dotted line on Bosart et al. (2000). The latter is starred to denote that it is computed as a difference between two layer averages (950–700 and 350–150 mb).

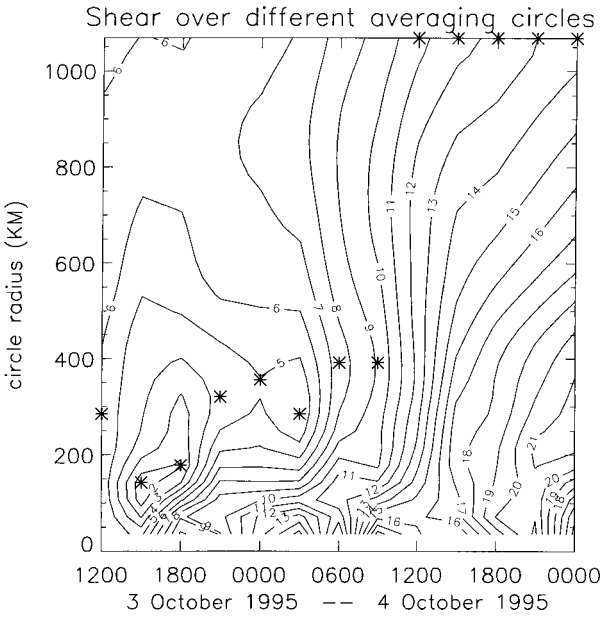

FIG. 7. Vertical wind shear (m s^{-1}) across the 850–200-mb layer testing sensitivity to the exterior radius of the averaging circle. Stars denote the shear measure at each analysis time with a minimum value.

over 5 m s^{-1} after 1200 UTC 4 October 1995 in a limited layer near 200 mb. The role that an environmental wind that changes direction with height can have on storm intensity is not clear. This layer strongly affects the 850–200-mb shear measure (Fig. 8, solid), but moderately affects the other two shear measures defined above and below 200 mb. Variations in the storm-parallel component of environmental wind strongly influence the 850–250-mb shear measure prior to 1200 UTC 4 October and accounts for the larger magnitude of this measure relative to the 850–200-mb measure. Opal stops intensifying at 1200 UTC 4 October, and after this time the storm can be considered strongly sheared with values approximately 13 m s^{-1}. This shear can be attributed to the southward and eastward progression of the jet stream (not shown) is response to the synoptic-scale trough. For context, a conventional hodograph plot of the environmental flow for a strengthening and weakening stage is shown in Figs. 10a and 10b, respectively. In the latter figure, the narrow layer of left-to-right shearing (relative to storm motion) can be seen.

The variations in environmental shear appear coincident with changes in the intensification rate within the GFDL model, despite the use of a moist convective adjustment parameterization whose responsiveness to increased shear is not clear and despite the coarse resolution (15 km) of the model integration. Two distinct events of lowered shear between 1500 and 1800 UTC 3 October and at 0300 UTC 4 October are coincident or slightly precede intensification events (Fig. 3). The eventual end to intensification, while not weakening as the observed storm did, is associated with both a long-term trend for increasing environmental shear (Fig. 6) and with a sudden shift in the character of environmental flow (Fig. 7) such that a minimum in analyzed shear at intermediate radii (~300 km) is no longer present.

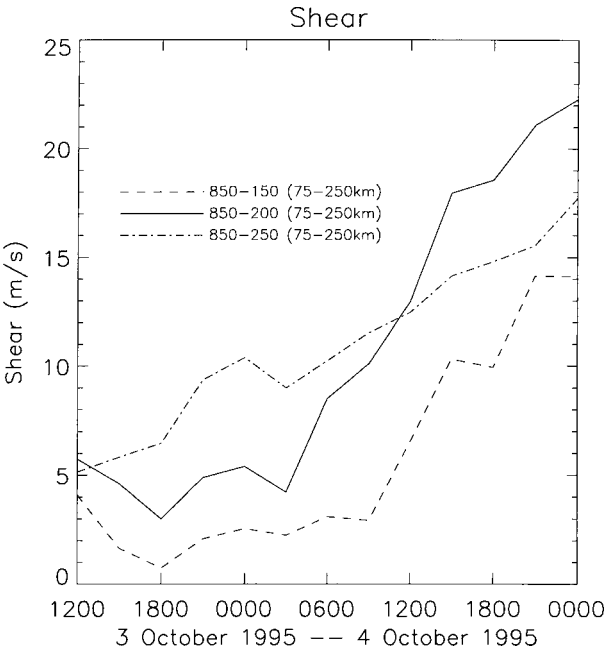

FIG. 8. Vertical wind shear measures testing sensitivity to selection of analysis layers.

b. Mean tangential momentum budget

A mean tangential momentum budget is constructed by casting the equations of motion into cylindrical coordinates, subtracting the storm motion vector from the wind, and finding azimuthal means (and asymmetries) of all quantities. Denoting the tangential wind by v, the radial wind u, and the vertical p velocity by ω, the tendency of the mean tangential wind can then be written as the sum of four terms, plus a friction term:

$$\underbrace{\frac{\partial \overline{v}}{\partial t}}_{\substack{\text{tangential}\\ \text{wind}\\ \text{tendency}}} = \underbrace{-\overline{u'\zeta'}}_{\substack{\text{eddy}\\ \text{vorticity}\\ \text{flux}}} + \underbrace{-\overline{u}\,\overline{\zeta}}_{\substack{\text{mean}\\ \text{vorticity}\\ \text{flux}}} + \underbrace{-\overline{\omega'\frac{\partial v'}{\partial p}}}_{\substack{\text{eddy}\\ \text{vertical}\\ \text{advection}}} + \underbrace{-\overline{\omega}\frac{\partial \overline{v}}{\partial p}}_{\substack{\text{mean}\\ \text{vertical}\\ \text{advection}}} + \text{Friction}, \tag{1}$$

where ζ is the vertical absolute vorticity, overbars represent azimuthally averaged quantities, and primed quantities are deviations from that average. The friction term is computed using

$$\text{Friction} = p_{\text{sfc}}^{-1}[-\sin\theta({}_{\text{H}}F_x + {}_{\text{V}}F_x) + \cos\theta({}_{\text{H}}F_y + {}_{\text{V}}F_y)], \tag{2}$$

where p_{sfc} is the surface pressure, θ, is the counterclockwise azimuth angle from east, ${}_{\text{H}}F_x$ and ${}_{\text{H}}F_y$ are components of the frictional force due to lateral stress, and ${}_{\text{V}}F_x$ and ${}_{\text{V}}F_y$ are components of the frictional force due to vertical stress (explained in detail in Kurihara and Tuleya 1974). Left out of this budget is the small beta term $[\beta r \sin\theta(u' + c_r)]$, where c_r is the radial component of the storm motion vector. With asymmetries on the order of 5 m s^{-1}, simple scale analysis suggests this term can provide for a 5 m s^{-1} day^{-1} tendency beyond a radius of 600 km, but in practice the in-phase relationship delays the importance of this term to further radii.

The tangential wind budget is then computed for a time of rapid intensification (1800 UTC 3 Oct 1995) and a pause in intensification (0000 UTC 4 Oct). The temporary pause still occurs within the long-term trend for intensification of Opal within the model and occurs before the onset of shear at later times in the simulation (Figs. 3 and 9). The resulting tendencies in the r–p plane are displayed in Figs. 11 and 12, respectively. At the intensifying time, the total mean tangential wind tendency computed from the budget (Fig. 11f) shows a vertically coherent tendency for spin up at the eyewall from just above the ground to 320 mb, while the nonintensifying total budget tendency (Fig. 12f) has no such coherent structure, alternating between positive and negative tendency with height. At different vertical levels, different terms contribute to produce this coherent maximum in total tendency at the time of intensification. At that time, 1) the lowest levels (~850 mb) show a less negative eddy vorticity flux (Fig. 11a vs. Fig. 12a) and a stronger eddy vertical advection (Fig. 11c vs Fig. 12c) relative to the nonintensifying time, 2) from 600 to 400 mb the eddy vertical advection is less negative (Fig. 11c vs Fig. 12c) and mean vorticity flux becomes a strong positive (Fig. 11b vs Fig. 12b), 3) above 400 mb the mean vertical advection is up to 40 m s^{-1} day^{-1} larger (Fig. 11d. vs Fig. 12d; difficult to discern in the figures presented here, but noticeable in difference plots) and the eddy vorticity flux is less negative (Fig. 11a vs Fig. 12a), and 4) the friction is weaker throughout the eyewall by about 10 m s^{-1} day^{-1} (Fig. 11e vs Fig. 12e). Many of these properties (greater vertical extent of positive tendency plus a reduction of negative eddy vorticity flux and enhancement of mean vorticity flux and mean vertical advection aloft) are consistent with a greater vertical extent of convection, suggestive of the Titley and Elsberry 1999 hypothesis, but examination of the vertical motion field (not shown) at these levels is less than convincing. Other features observed in the total budgets of mean tangential wind tendency are 1) the apparent spindown tendency in the boundary layer at intensification (Fig. 11f), and a spinup at nonintensification (Fig. 12f), and 2) the enhanced middle-troposphere spinup (Fig. 11f) at radii of 200 to 800 km from the storm as a result of enhanced mean vorticity flux (Fig. 11b) at intensification. Composite averages (not shown) of multiple intensifying and multiple weakening times show that tendencies near the center of storm are robust, but in the far field there is more variation.

The eddy vorticity flux at 200 mb is presented as a function of radius and time in Fig. 13. Of note is the region of positive eddy vorticity fluxes exterior to the 400-km radius, with negative values within. Titley and Elsberry (1999) proposed a preconditioning phase where eddy vorticity fluxes aloft provide a large-scale cyclonic environment at 200 mb that preceded rapid intensification of Typhoon Flo (1990). They hypothesize that a more cyclonic environment aloft will lower the shear above a cyclonic vortex. During their analyzed rapid intensification phase, the eddy vorticity fluxes are weak and largely negative. In the Opal simulation considered here, the intialization is too late to test the preconditioning hypothesis, but throughout the simulation the eddy vorticity fluxes are more characteristic of the preconditioning phase of Titley and Elsberry (1999). In that phase, they showed eddy vorticity fluxes peaking at intermediate radii (400–1200 km; here, 400–800 km) with values of ~20 m s^{-1} day^{-1},

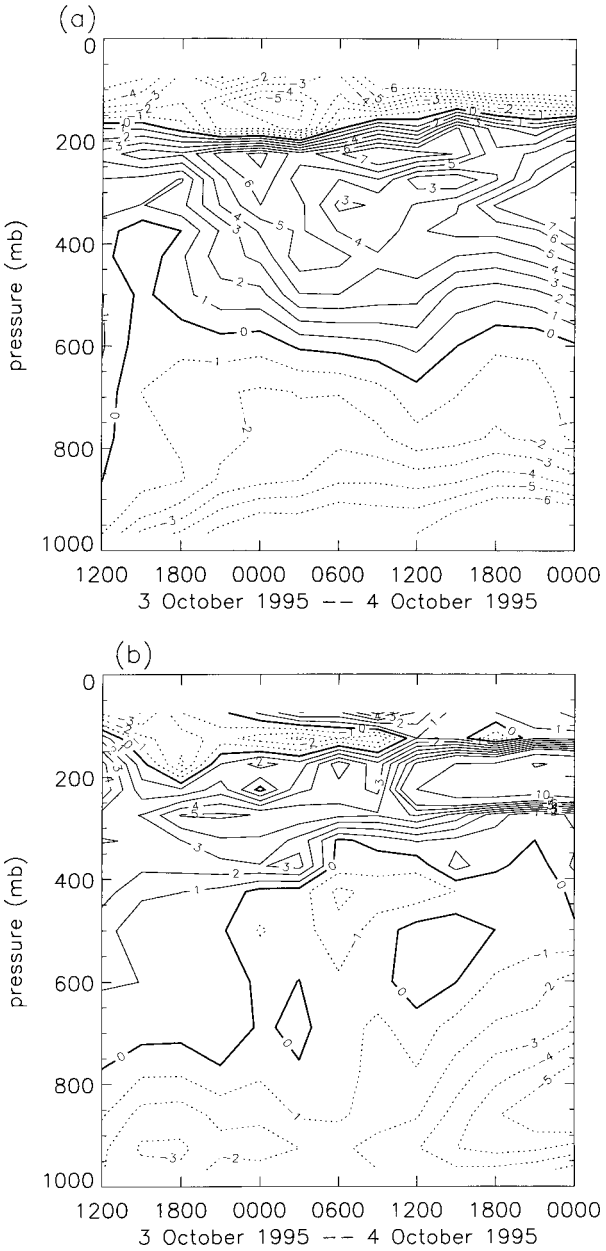

FIG. 9. The mean component of the environmental wind (m s^{-1}) using an averaging annulus of radii 75 and 250 km, (a) in the direction of storm motion with the storm motion subtracted, and (b) in the direction perpendicular to storm motion with winds from left to right (roughly from west to east) being positive. Contours are at a 1 m s^{-1} interval to 7 m s^{-1}, then at 10 and 15 m s^{-1}.

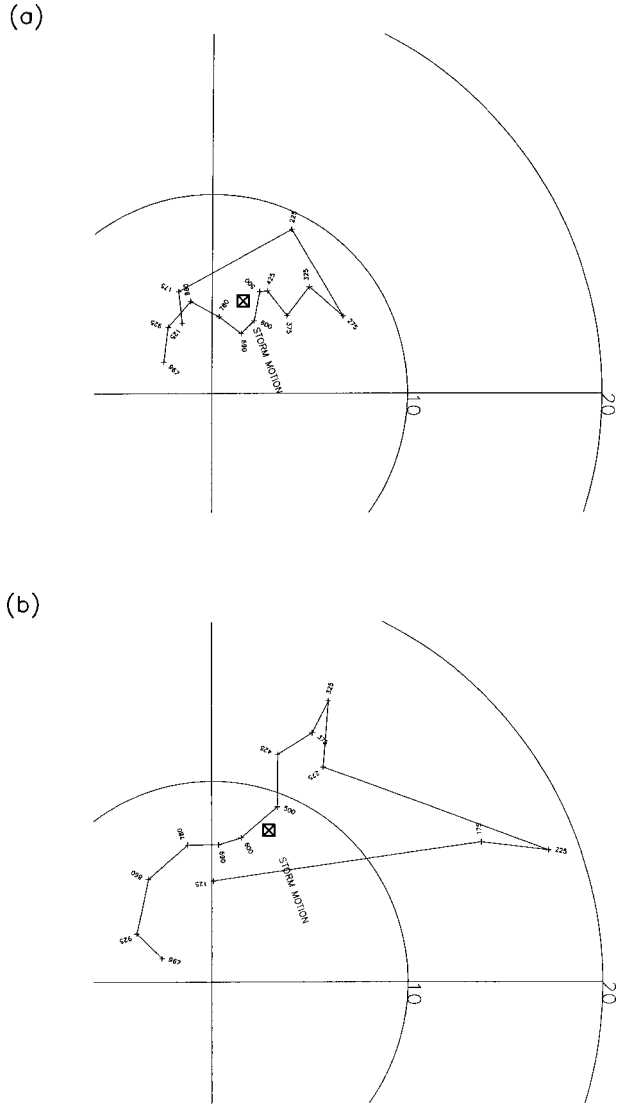

FIG. 10. Hodographs of the environmental wind within an averaging annulus of radii 75 and 250 km at (a) 1800 UTC 3 Oct and (b) 1800 UTC 4 October 1995. The circles represent vector magnitudes of 20 and 10 m s^{-1}. The storm motion vector is depicted by a crossed box.

similar to that found in Fig. 13. It is found though in the GFDL Opal simulation that the mean eddy vorticity flux exhibited vertical structure, with much of the signal to be found above 200 mb (Figs. 11a, 12a), so the choice of level may vary substantially from storm to storm. There is no evidence of large-scale cyclonic circulation at this level (Fig. 14), with cyclonic circulation confined to within approximately 400 km, comparable with the rapid intensification phase of Typhoon Flo (Titley and Elsberry 1999).

There is a suggestion for inward propagation of eddy vorticity flux in Fig. 13 with enhanced values ($>$10 m s^{-1} day^{-1}) appearing outside of the 600-km radius before 0300 UTC 4 October 1995, then inside of the 500-km radius around 1200 UTC 4 October. Molinari and Vollaro (1989) proposed such a signature for trough interaction in the development of Hurricane Elena. Given the track errors of this simulation, it is difficult to conclude that this process did not contribute to the intensification of the real storm, but the influences of eddy momentum forcings on the model storm can be examined within the Eliassen (1952) balanced vortex formulation, similar to ex-

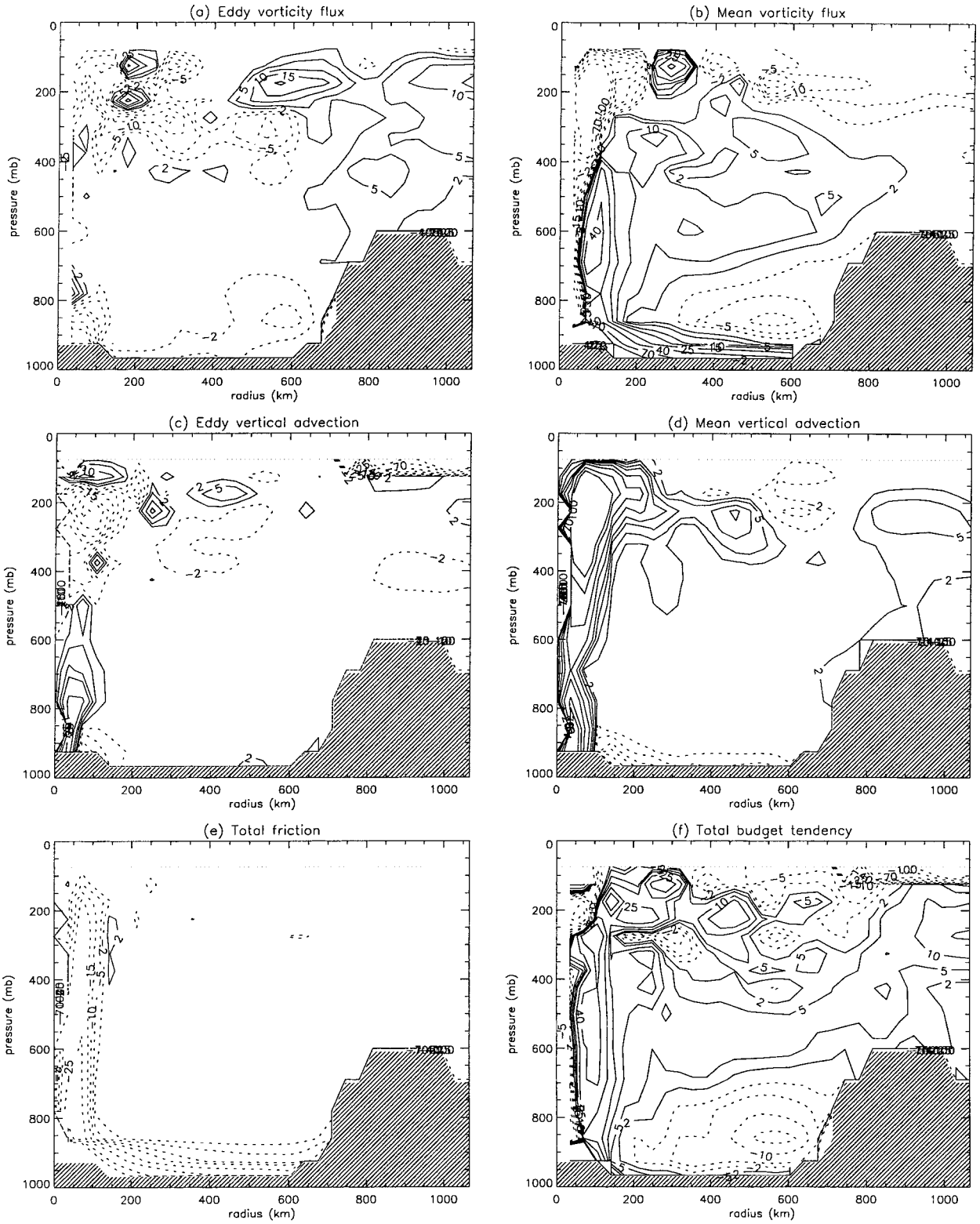

FIG. 11. The terms of the mean tangential wind budget equation at 1800 UTC 3 Oct 1995: (a) eddy vorticity flux, (b) mean vorticity flux, (c) eddy vertical advection, (d) mean vertical advection, (e) total friction, and (f) total of the five terms. The contours used are ±2, 5, 10, 15, 25, 40, 70, and 100 m s^{-1} day^{-1}. Dashed contours represent negative tendency for mean tangential wind.

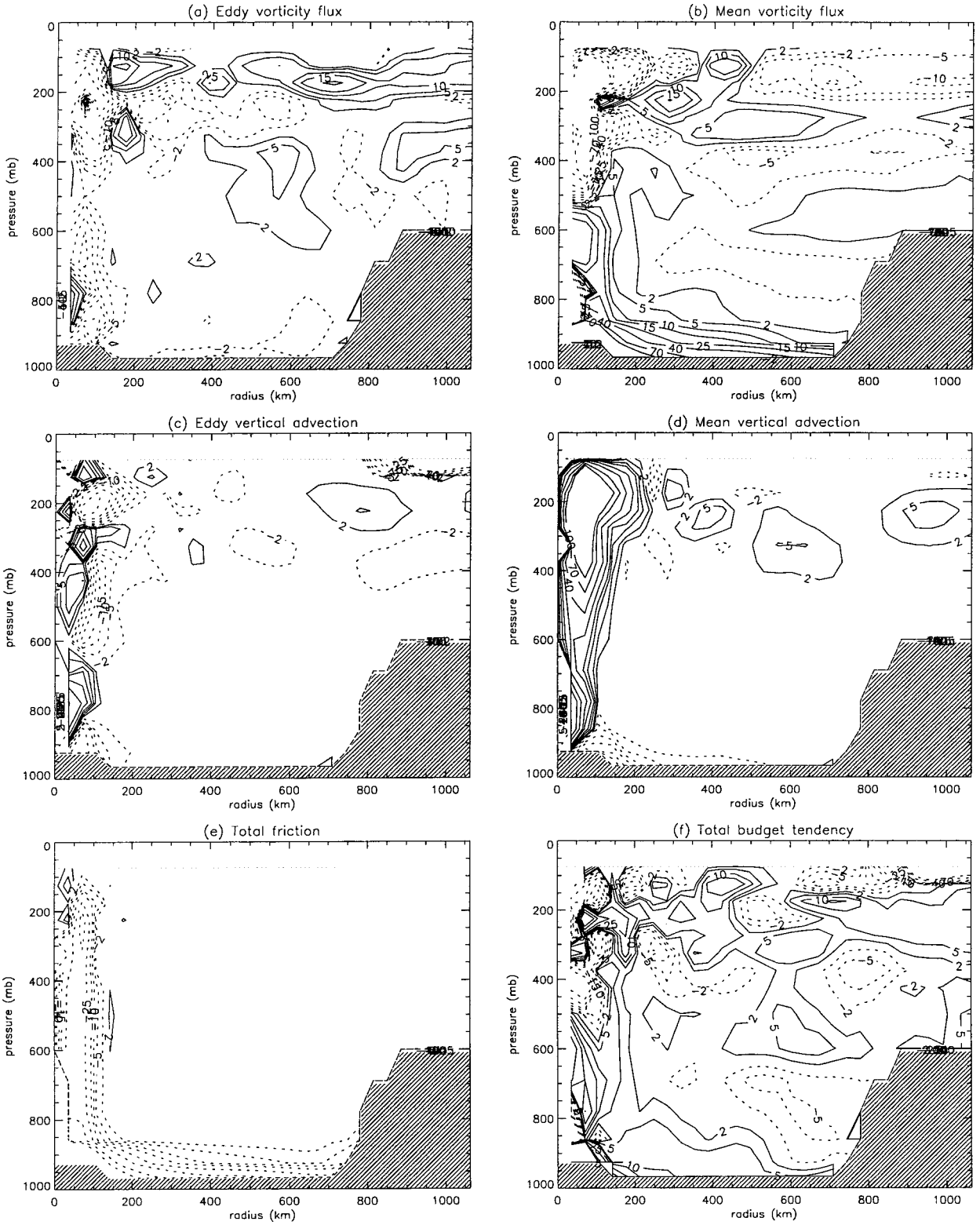

FIG. 12. The terms of the mean tangential wind budget equation at 0000 UTC 4 Oct 1995: (a) eddy vorticity flux, (b) mean vorticity flux, (c) eddy vertical advection, (d) mean vertical advection, (e) total friction, and (f) total of the five terms. The contours used are ±2, 5, 10, 15, 25, 40, 70, and 100 m s^{-1} day^{-1}. Dashed contours represent negative tendency for mean tangential wind.

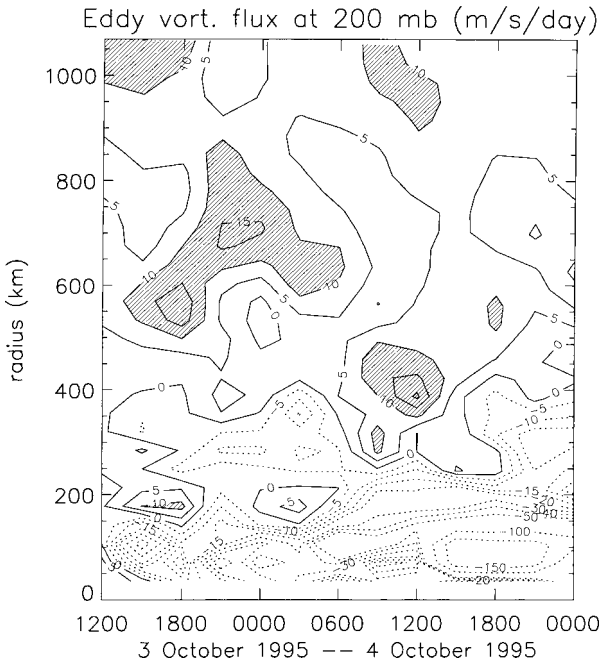

FIG. 13. Eddy vorticity flux (m s^{-1} day^{-1}) at 200 mb as a function of radius and time. This is computed as an average of the 175- and 225-mb layers and azimuthal means are displayed. Shaded areas denote a greater than 10 m s^{-1} day^{-1} tendency.

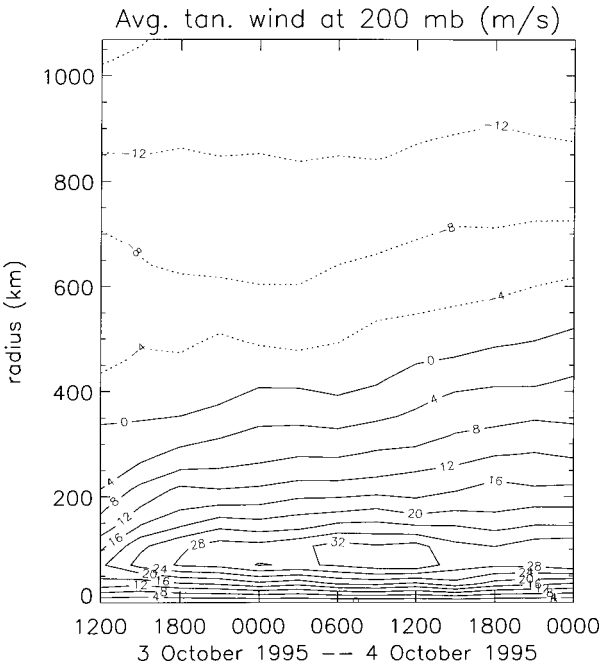

FIG. 14. Azimuthal mean tangential wind (m s^{-1}) at 200 mb as a function of radius and time.

aminations by Molinari and Vollaro (1989) and subsequent papers.

Our computation uses a pseudoheight vertical coordinate (Hoskins and Bretherton 1972), requiring reinterpolation of the dataset from the original rectilinear, σ coordinate to pseudoheight with a fixed 400-m vertical grid spacing, then interpolation to a cylindrical grid. The linearity of the elliptic partial differential equation for the mean transverse streamfunction driven by heat and momentum forcing allows us to consider the total balanced response as a superposition of separate source mechanisms for forcing over separate, arbitrary, mutually exclusive subdomains. To a first approximation, the mean secondary circulation and the attending mean tendency terms in the tangential momentum and heat budgets arise to counteract the mean diabatic heating in the eyewall and surface drag in the boundary layer so that thermal wind balance of the vortex is maintained (Willoughby 1979; Shapiro and Willoughby 1982). Consistent with the recent balanced diagnosis of this storm by MS, we have found that the mean diabatic heating rate associated with the latent heat release in the eyewall accounts for the mean tendency terms in the tangential momentum budget (not shown). Moreover, the variability in the mean terms appears to be governed by variability in the heating rate. Further discussion of this quantitative calculation is presented in MS.

We use the Eliassen model to examine the influence of the trough on the storm by taking the azimuthal mean static stability and primary circulation to define the vortex, considering all heat forcings to vanish, and considering the eddy flux of vorticity as the only momentum forcing. We confine the forcing to that plausibly associated with the trough by having all the eddy vorticity fluxes interior to the 400-km radius vanish. The resulting secondary circulations and net tangential wind tendency (the original eddy flux forcing plus that inferred from the response of the balanced vortex) for intensifying and nonintensifying phases are shown in Fig. 15. Net tendencies largely remain outside the 400-km radius and the induced secondary circulations at the eyewall are very weak ($w \lesssim 1$ mm s^{-1}). According to this calculation the eddy flux forcing by the trough has only a negligible influence on the storm during both intensifying and nonintensifying phases. A second computation setting the static stability within the eyewall to a low value (one-half the value derived from the model basic state, 1×10^{-4} s^{-2}), acknowledging the ease of vertical motions there because of the convective feedback (Emanuel et al. 1987; Montgomery and Farrell 1993), produces nearly identical circulations and forcing. Based on these calculations, the hypothesized benefit of trough interaction does not appear to be supported in this simulation.

c. Upper-level divergence

Operational surface analyses performed by NCEP show a surface trough over Louisiana, Mississippi, and Alabama from 1200 UTC 3 October to 0000 UTC 4 October 1995, which moves eastward after that (not shown). The surface

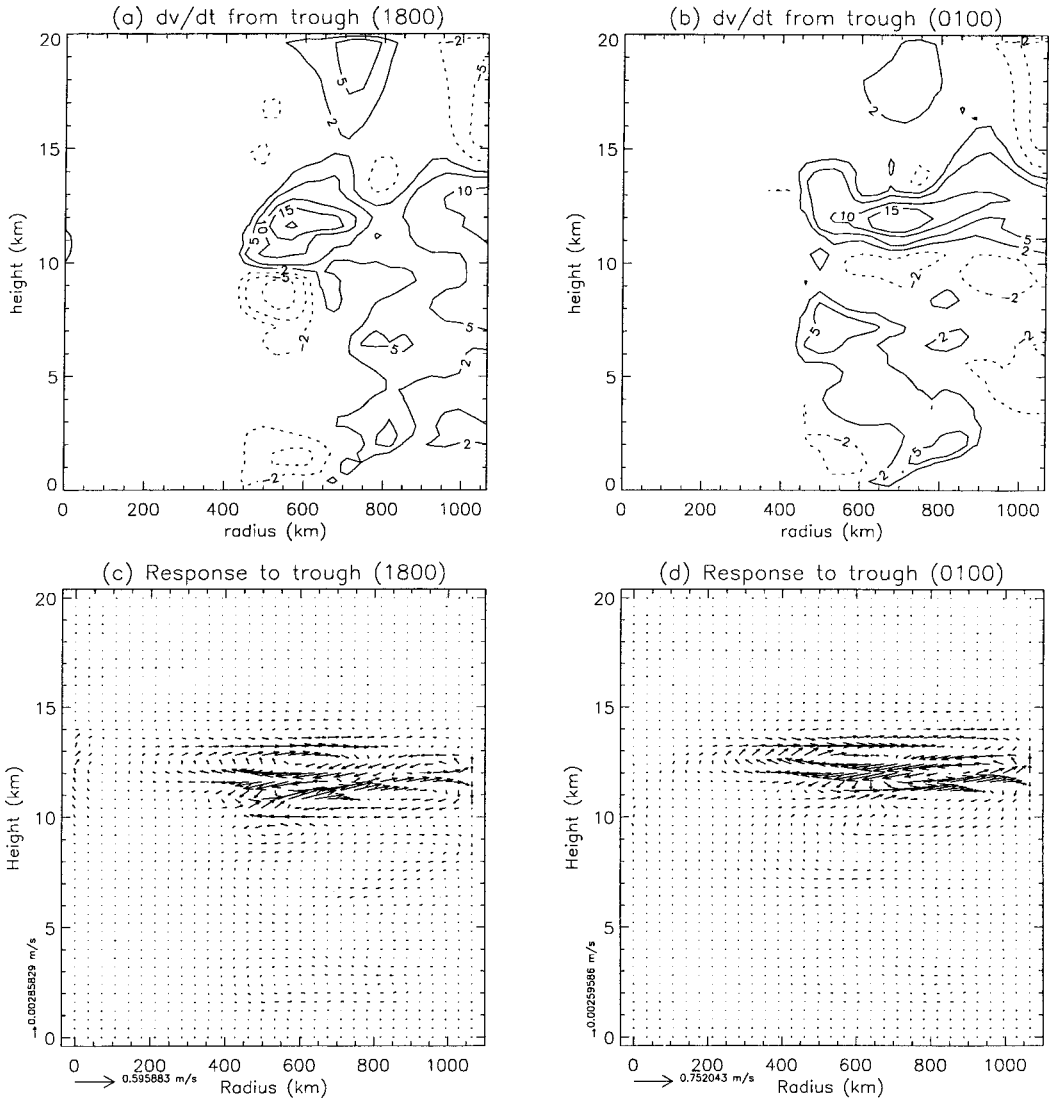

FIG. 15. The tendency of mean tangential wind due to eddy vorticity fluxes exterior to a radius of 400 km and from the resulting Eliassen balanced vortex response of the same for (a) 1800 UTC 3 Oct and (b) 0100 UTC 4 Oct 1995. Also shown in (c) and (d) are the corresponding secondary circulations resulting from the same forcings, respectively. Maximum vector components are noted on either side of the origin.

trough is associated with heavy rain and thunderstorms. The GFDL simulation reproduces aspects of this feature, with upward motions evident over the same region (Figs. 16a–c, label A). The convective line is the northern end of a long (~2000 km), deep (up to 600 mb), southerly fetch of moist air. Opal then traverses this warm maritime air mass as it heads north. Generally associated with this feature is an enhancement in absolute vorticity (Figs. 17a,d,g, label A) at the 925-mb level slightly to the west of its position. A vertically stacked vorticity structure extends to the southwest from the mouth of the Mississippi River at 0300 UTC 4 October (Figs. 17g,h,i, label B). Enhancement of 200–300-mb mean layer divergence (Fig. 18) to $\sim 5 \times 10^{-5}$ s^{-1} in this vicinity (labels A in Figs. 18a–c and B in Fig. 18c) is generally collocated with the vertical velocity pattern at lower levels, especially over land. These upper-level divergences correspond roughly to the same computation of B00 (their Figs. 6–8) using satellite-enhanced data assimilation procedures, except in the near vicinity (~300 km) of the hurricane center. Near 1800 UTC 3 October (close to Fig. 18a), both analyses show a broad maximum over Alabama (label A) with similar magnitude, and extension of positive divergence toward the eastern Gulf of Mexico and Florida (label D). The GFDL forecast, however, produces an approximately stationary positive divergence maximum over the southern tip of Texas (Figs. 18a–c, label C) that the satellite-based analysis did not capture. At 0000–0300 UTC 4 October, the satellite-based analysis pulls the former divergence maximum (label A) further northeast from Alabama to

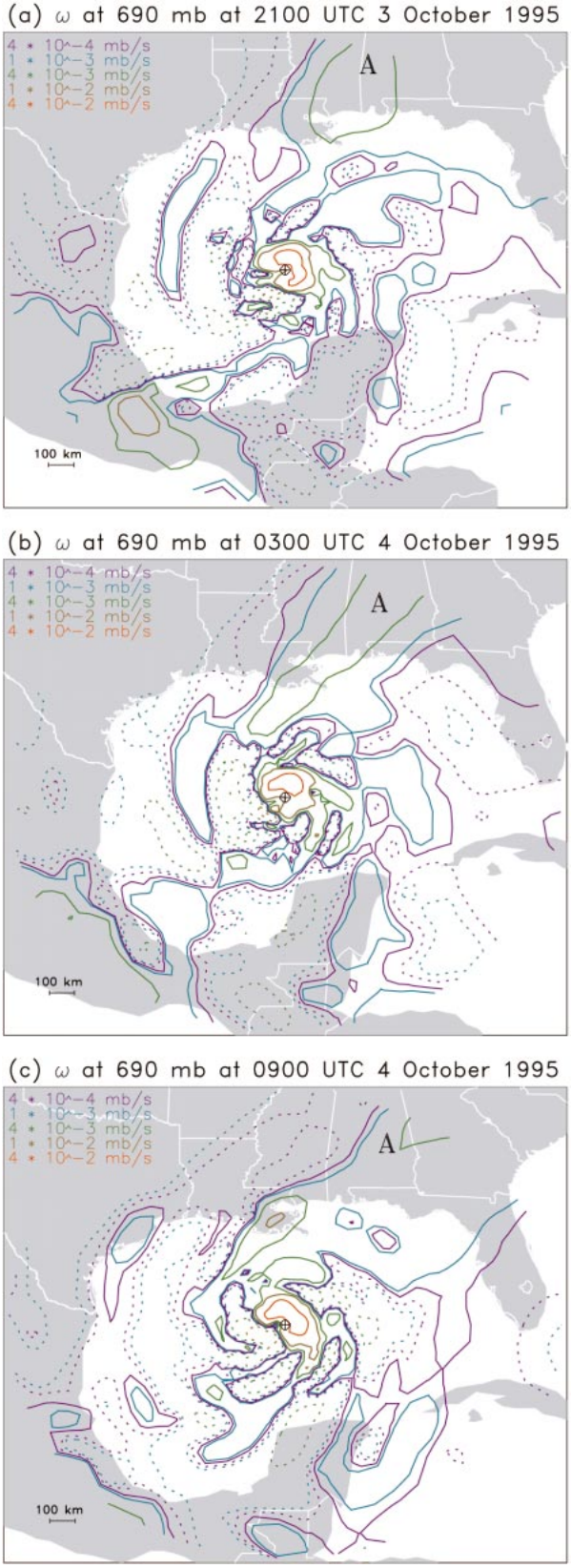

Tennessee (extending to label E in Fig. 18b). There is less of this tendency in the GFDL forecast (Fig. 18b, perhaps as a result of the limited analysis domain presented here), but both analyses show divergence values around 2×10^{-5} s^{-1}. At 0900–1200 UTC 4 October, both analyses pick up on a north–south-aligned convergence feature (Fig. 18c, label F) over eastern Texas with a peak in divergence (label B) near the mouth of the Mississippi River, and weaker divergences extending to the northeast. Noting this correspondence between the GFDL model-derived and satellite wind-enhanced divergence fields away from the storm, the GFDL model output may be able to test the hypothesis advanced by B00 (p. 347) that *this divergence feature helped "trigger the areal expansion of deep eyewall convection" in the first stage of intensification*, beginning in their analysis at 1500 UTC 3 October.

In the GFDL analysis, the divergence collocated with the trough north and west of the storm (with values from $\sim 5 \times 10^{-5}$ s^{-1} to $\sim 7 \times 10^{-5}$ s^{-1} in Figs. 18a–c) is never contiguous with the much stronger divergence ($\sim 1 \times 10^{-3}$ s^{-1}) associated with the hurricane itself at this level (small crosshairs at the center of each panel). From examination of the vertical structure of the divergence and the radial and vertical flow (Fig. 19), we can see that the divergence and outflow pattern associated with the hurricane emerges above 200 mb. Furthermore, the most significant divergence features to the north (i.e., to the left of Fig. 19) are evident at lower levels. These lower-level divergence features appear to mark the upper boundary of a region of upward motions far removed from the center of the hurricane, associated with the convective line over Louisiana. The degree of correspondence between the upper-level divergence pattern and the upward motions of the convective line suggests that the upper-level divergence is primarily responsible for (or primarily a reflection of) the convection over Louisiana. Given the assumption that the GFDL model reasonably simulated this aspect of the hurricane, it does not appear that the divergence aloft in the vicinity of the jet entrance region promoted extra lifting in the eyewall. In plan-view plots of the eddy quantities that contribute to the mean tangential wind budget (not shown), there is no noticeable contribution to storm intensification via the convective line.

d. Simulated vertical motions

Noticeable in the plan-view plots of vertical motions (ω, Fig. 16) is the systematic tendency for peak upward

←

FIG. 16. Vertical velocities, $\omega = dp/dt$, in terms of mb s^{-1} at (a) 2100 UTC 3 Oct (b) 0300 UTC 4 Oct, and (c) 0900 UTC 4 Oct 1995. The magnitudes of contours are listed in the legend. The sense of the contours are reversed, so that solid contours are upward (negative dp/dt) motions, and dashed are downward (positive dp/dt) motions. The crosshairs mark the center of the storm. The label A is explained in the text.

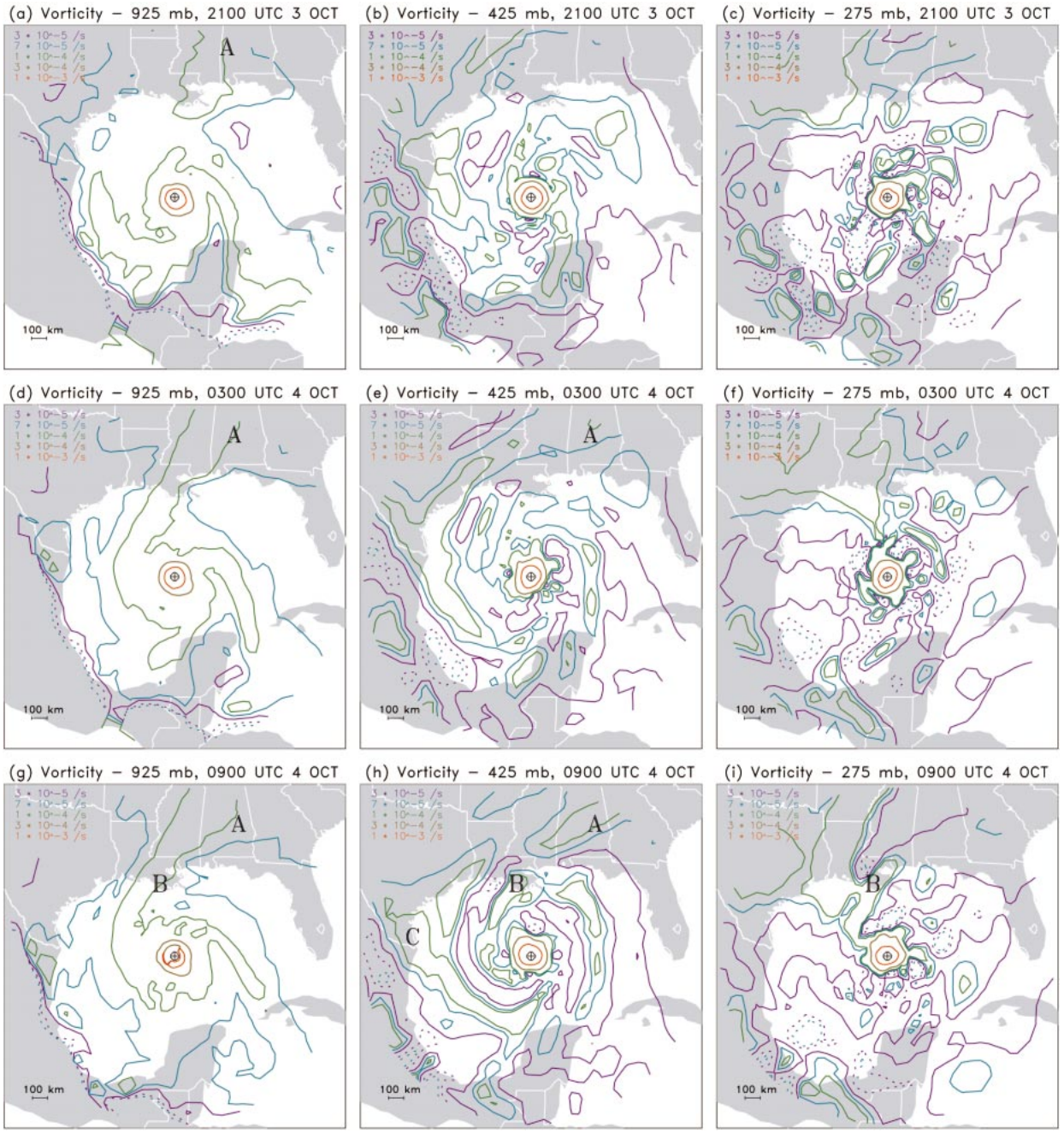

FIG. 17. Absolute vertical vorticity at 1800 UTC 3 Oct at (a) 925 mb, (b) 425 mb, and (c) 275 mb; at 0300 UTC 4 Oct at (d) 925 mb, (e) 425 mb, and (f) 275 mb; and at 0900 UTC 4 Oct 1995 at (g) 925 mb, (h) 425 mb, and (i) 275 mb. The magnitudes of contours are listed in the legend. Dashed contours are negative. Crosshairs mark the center of the storm. The labels A, B, and C are explained in the text.

motions to lie just to the north of the storm (in front of the moving storm center). Also of note is the trend with time for downward motions in the southwest sector of the storm. To summarize these tendencies and to expose other trends in near-storm vertical motion, an analysis is performed on each azimuth from the center of the storm in the *r–p* plane to find the peak upward motion (PUM) and peak downward motion (PDM) within the analysis grid. The analysis is limited to the first eight radial grid points (to ~250 km) and is representative of the grid-scale (coarse grain) response of storm vertical motions in the model near the hurricane. Taken together, the PUMs (and PDMs) define a set of 60 elements computed on each of the 60 azimuths. Figure 20 presents a summary of these samples as a function of time.

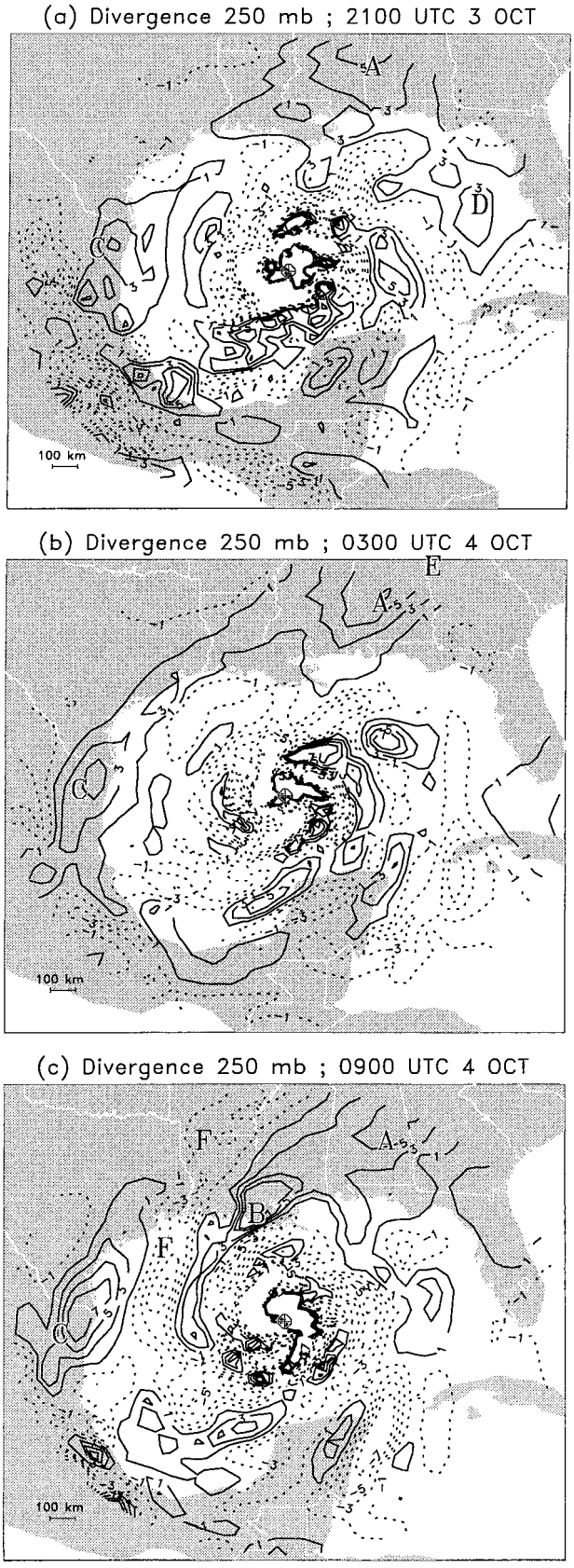

The mean PUM remains (Fig. 20b) about -0.07 mb s^{-1} (1 m s^{-1}) through most of the simulation, but the mean altitude of PUM (Fig. 20f) gradually descends from 400 to 600 mb with greater intensification episodes (1800 UTC 3 Oct and 0600 UTC 4 Oct, see Fig. 3) loosely associated with lower altitudes of mean PUMs and higher variance of PUM (i.e., enhanced convective asymmetry; Fig. 20d). The final episode of high PUM variance is not associated with storm intensification and occurs after the onset of strong shear (Fig. 6). Given the near-constant mean in PUM, an increase in PUM variance is associated with an increase of extreme values of PUM (Fig. 20b, dotted). Generally, lower-altitude and more extreme upward motions may intensify the circulation of the storm through enhanced vortex stretching. If the third of the sample of PUMs (20 elements) that have the most extreme value is considered, there appears to be a transition after the onset of shear such that the altitude of these PUMs falls below that of the single strongest PUM (Fig. 20f, dashed vs dotted). Observations of a weakening, sheared hurricane (Reasor et al. 2000) show a localized increase combined with a lowering of altitudes of upward motions, so this signal can be associated with both enhanced intensification (as realized in this model) and imposed shearing (both in the model and in theory). Both the extreme and mean PDMs (Fig. 20a) increase gradually throughout the simulation, although of an order of magnitude smaller than the PUMs. While the altitude of mean and extreme PDMs (Fig. 20e) show mixed trends through the simulation, of note is the inward migration of extreme PDMs toward the center of the storm (Fig. 20g), particularly after 1500 UTC 4 October when the storm has stopped intensifying. These latter PDMs exist at the same radius as the PUMs (Fig. 20h), lying within the eyewall.

The vertical motion pattern observed in Fig. 16 is typical of the downshear enhancement of upward motion shown by observations (Reasor et al. 2000) and modeling studies (downshear and to the left in Frank and Ritchie 1999). This pattern is present more or less throughout the simulation, without predictive value for the model storm. The PUMs highlight variations in convection during intensification, pauses during intensification, and highly sheared phases. Combined with PDM variance and radius, the different phases can be identified. The variations of the most intense subsample (here the most extreme third is used) appear to have the best diagnostic value.

←

FIG. 18. Divergence of the horizontal wind averaged between the 225 and 275-mb layers at (a) 2100 UTC 3 Oct, (b) 0300 UTC 4 Oct, and (c) 0900 UTC 4 Oct 1995. The contours displayed are $\pm(1, 3, 5, 7) \times 10^{-5}$ s^{-1}, with only the leading digit shown. Dashed contours are convergent. Crosshairs mark the center of the storm. Letter labels are explained in the text.

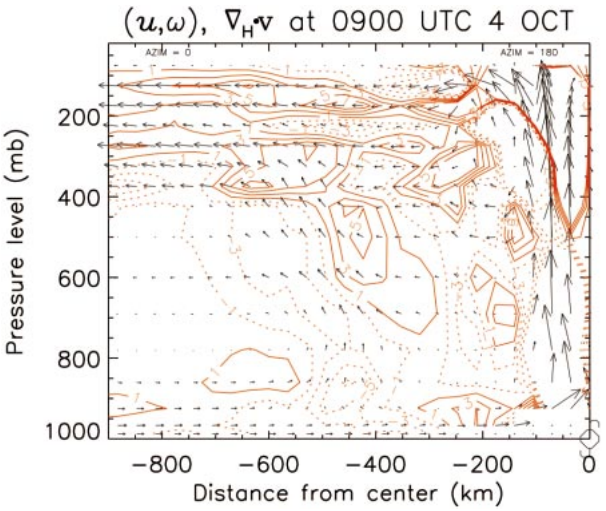

FIG. 19. Vertical cross section of radial and vertical winds and divergence at 0300 UTC 4 Oct 1995, where the left edge is at 10° azimuth (just east of north). The hurricane center is at the right of the cross section. The maximum vector represents approximately 26.4 min of translation, i.e., 89 m s^{-1} radially and 524 mb h^{-1} vertically. The contours of divergence are at $\pm(1, 3, 5, 7) \times 10^{-5}$ s^{-1}. Dashed contours are convergent.

4. Discussion

Studies of the role of environment in rapid hurricane intensification fall basically into two classes: 1) studies where given a benign (i.e., nonhostile), uniform environment, the hurricane reaches maximum intensity (''hostile environment'' theories), and 2) studies where an environmental influence is advected into the proximity of the hurricane core to promote intensification (''stimulating environment'' theories). Both classes rely on the ability of convection to aid intensification through midlevel inflows that conserve angular momentum or through stretching of the ambient vorticity field at low levels.

a. ''Hostile environment'' theories and modeling

Shear-based theories relate storm intensification to a reduction of vertical shear. Increased shear is hypothesized to ventilate a pocket of warm air aloft away from the eye of the hurricane, leading to an increase in surface pressure (Gray 1968), or to tilt a balanced vortex such that the thermal field consistent with it is altered and affects the stability of convection (DeMaria 1996; Jones 1995). Using 850–200-mb shear as a traditional measure of shear across a hurricane (Fig. 6), the Opal simulation shows a low value of shear ($<$10 m s^{-1}, the threshold identified by B00) throughout the period of intensification (to 1200 UTC 4 Oct 1995; Fig. 2). Figure 9, though, provides a more complicated picture. The mean flow at 850 mb is less than 2 m s^{-1} in both components of the flow, so most of the variability in shear is determined by the environmental winds aloft. Interestingly, 200 mb lies above the level of greatest storm-relative winds prior to 1200 UTC 4 October 1995 (i.e., through the period of intensification). Therefore, if a slightly different shear measure is selected (e.g., 850–250 mb) Hurricane Opal would appear to be highly sheared, with values approaching 10 m s^{-1} near 0000 UTC 4 October 1995 (Fig. 8). So while the shear environment prior to 1200 UTC 4 October 1995 was more beneficial to storm intensification than after that time, it should not be called an especially benign shear environment. The details of the imposed environmental winds appear to be important. Between 2100 UTC 3 October and 0900 UTC 4 October, the perpendicular component is weak through the model atmosphere, with values confined between -3 and 5 m s^{-1}. After this time, a very strong left-to-right component of the mean wind up to 15 m s^{-1} is felt above 250 mb. A Green function technique is used to find the horizontal streamfunction and velocity potential at a particular level by respectively inverting the vorticity and divergence fields from that level. After the subsequent computation of rotational and divergent winds, it is found that the primary component of the introduced shear aloft is in the residual wind field (i.e., the difference between the total wind and the combined rotational and divergent wind). Such a residual wind field would be due to the presence of vorticity or divergence sources outside the analysis domain of a 1000-km radius. Examination shows that this residual wind takes the form of a broad-scale deformation flow with a col point in the vicinity of the hurricane. The onset of perpendicular shear is coincident with a shift of the col point to the east off of the center of the hurricane. The component of shear parallel to storm motion (with the storm motion subtracted; Fig. 9a) is initially small, but soon after initialization (after 1800 UTC 3 Oct) the storm is sheared from the rear with an inflow of air at low levels from the front end (north end) of the storm, yet Opal still intensifies for the next 18 hours. A shear theory that seeks a simple numerical value between two levels is incomplete if it does not address particular arrangements of shear (twisting shear, shear relative to storm motion, shear confined in thin layers, etc.) and the role of a such complications to the intensity problem is not clear.

The maximum potential intensity theory of Emanuel (1995) is applied by B00 (their Fig. 21) to Hurricane Opal, suggesting that the lowering of MPI at later times interrupts the intensification of Opal. The modeling approach of Emanuel (1999) is an extension of this MPI theory, by including ocean interactions. The approach encapsulates the uniform, axisymmetric response of a hurricane to variations of surface heat exchanges with the ocean and to the thermodynamic profile of the ambient atmosphere. This type of forecast is dependent on an accurate track forecast. The influence of vertical shear is not accounted for in the Emanuel model and at times is used to explain inaccuracies in the forecast. Emanuel (1999) explains the initial intensification of Opal by the translation of the storm away from a pool of relatively cool surface water at the southern end of

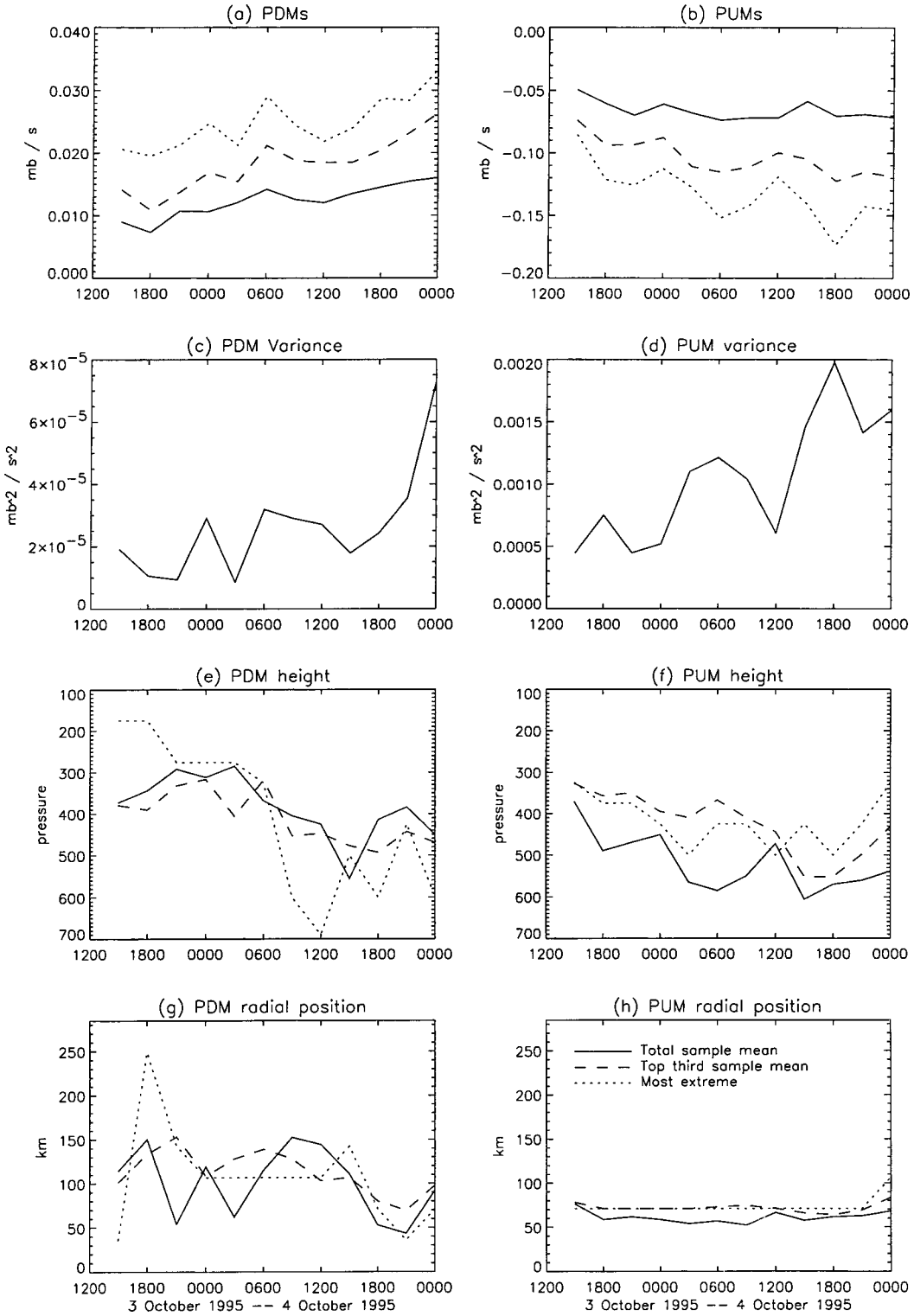

FIG. 20. Statistics derived from the samples of PDMs and PUMs, displayed as a function of time. Solid lines refer to the complete sample, while the dashed lines refer to the most extreme one-third of events and the dotted lines refer to the most extreme vertical motions. (a) PDM magnitude in mb s^{-1}, (b) PUM magnitude in mb s^{-1}, (c) variance of PDM, (d) variance of PUM, (e) pressure level of PDM, (f) pressure level of PUM, (g) radial position of PDM, and (h) radial position of PUM, plus legend.

the Gulf of Mexico (B00). The cold pool developed as a result of frictionally forced upwelling of the ocean caused by the surface winds of Opal as it stalled just west of the Yucatan Peninsula for two days (Bender and Ginis 2000; their Fig. 7). The current simulation is not able to address this because the cold pool is not present in the initialization. Figure 1 in Emanuel (1999) summarizes several of his Opal simulations, where the best forecast (with a pronounced maximum followed by a weakening prior to landfall) includes the effects of sea surface temperature plus the effects of the warm core ocean eddy. Without the effects of the WCE, the Emanuel model intensifies Opal more slowly, reaching peak intensity at landfall. Emanuel's conclusion is that variations in surface fluxes controlled the variations in intensity of Opal. The GFDL simulation also weakens Hurricane Opal (slightly) prior to landfall, but the sea surface temperatures in the model vary by only 1 K across the Gulf of Mexico and the WCE is not present. In the GFDL model, the onset of large vertical shear is coincident with end of the intensification of Opal. We are left with two computer models that can successfully produce the modulation of the intensity of Opal, yet for apparently different reasons. This is not to minimize the importance of the WCE, but rather to point out a modulation of intensity due to atmospheric sources not present in the Emanuel model.

b. ''Stimulating environment'' theories

Montgomery and Kallenbach (1997) showed how vorticity asymmetries excited near the eyewall of a hurricane tend to symmetrize via sheared vortex Rossby waves. By their Fig. 8, the wave–mean flow interaction leads to an acceleration of mean tangential winds near the original asymmetry, and a slowing of the mean tangential winds exterior to the acceleration region. Such a wave–mean flow momentum transfer would be realized in the mean tangential wind budget as oppositely signed forcings in the eddy vorticity flux term. The present study has found that near the storm center negative eddy vorticity fluxes slow the mean vortex circulation at both lower and upper levels at every time step (although with variations in magnitude at different times). It may be that, at the model resolution presented here, the negative forcings on mean tangential winds, which by theory occur at outer radii, are simply more apparent. However, within the present dataset the eddy vorticity flux is found to be dominated by the signature induced by the shear, with negative radial winds at the front end of the storm at low levels and negative radial winds at the back end of the storm aloft. Once this shear-induced eddy vorticity flux signature is quantified, the possible roles of smaller scale ($<$100 km) asymmetries may be addressed as in MS.

Beyond the inner core of the hurricane, vorticity asymmetries are also thought to aid intensification of a tropical cyclone (Challa and Pfeffer 1990; Molinari and Vollaro 1990). Because a vorticity asymmetry reflects that the hurricane is out of symmetric gradient wind balance, the vortex will try to restore balance by generating a secondary circulation. If a positive flux of eddy vorticity is introduced aloft, then balance can be restored by an outward wind at that level, which is associated with a negative tendency for the mean tangential winds. Since it is introduced aloft, the secondary circulation is completed by enhanced inflow below this level and enhanced lifting at radii interior to the asymmetry aloft. Positive eddy vorticity fluxes are analyzed in the present analysis exterior to the 400-km radius from the center of Hurricane Opal. Plan views of the eddy vorticity flux confirm their strong relationship with vorticity asymmetries aloft (i.e., Fig. 5). These results could suggest the importance of a reduction of scale of the vorticity features by a symmetrization process (e. g. Melander et al. 1987; Carr and Williams 1989; Smith and Montgomery 1995), which is more favorable for ascent without the negative impact of an increased shear (Molinari et al. 1998). The results of section 3b indicate that this is not important for Opal in terms of enhanced lifting, yet it still may prove important in terms of reducing the negative impact (i.e., vertical shear) of vorticity features of large horizontal scale.

5. Conclusions

Hurricane Opal traversed the Gulf of Mexico and intensified very rapidly. While the shear environment may not have been hostile to storm development, it was not especially benign either, so this is not an ideal candidate for low-shear intensification. The model hurricane, nonetheless, appeared to intensify as much as it could consistent with thermodynamic parameters of the problem (as illustrated by B00) up to a time defined by the onset of intense cross-vortex flows aloft. We suggest that the trough played a minimal role in intensification, supporting the model simulation of Emanuel (1999; cf. his Fig. 1) where no effects of the trough are included in his axisymmetric model.

Different mechanisms are proposed, though, for the *weakening* of Opal by Emanuel (a decrease in ocean heat content) and by this paper (an increase in shear), which raises a scientific dilemma. We propose that the sensitivity of both storm intensification and weakening in the model may be tested by removing the trough from the initial data fields, reinitializing the model, and then analyzing the model output.

Acknowledgments. This work was supported by ONR Grant N00014-93-1-0456 P00006 and by Colorado State University. We would like to thank Drs. P. Reasor, D. Nolan, and J. R. Gyakum for their critical reviews, and to thank J. P. Camp, Dr. L. Bosart, Dr. W. Gray, T. Cram, and J. Fulton for enlightening conversations. The computer support of Rick Taft, Janice Enagonio, and Sam Grandlienard is also acknowledged.

REFERENCES

Bender, M. A., 1997: The effect of relative flow on the asymmetric structure in the interior of hurricanes. *J. Atmos. Sci.,* **54,** 703–724.

——, and I. Ginis, 2000: Real-case simulations of hurricane–ocean interaction using a high-resolution coupled model: Effects on hurricane intensity. *Mon. Wea. Rev.,* **128,** 917–946.

Black, M. L., and J. L. Franklin, 2000: GPS dropsonde observations of the wind structure in convective and non-convective regions of the hurricane eyewall. Preprints, *24th Conf. on Hurricanes and Trop. Meteorology,* Fort Lauderdale, FL, Amer. Meteor. Soc., 448–449.

Bosart, L. F., and J. Bartlo, 1991: Tropical storm formation in a baroclinic environment. *Mon. Wea. Rev.,* **119,** 1979–2013.

——, C. S. Velden, W. E. Bracken, J. Molinari, and P. G. Black, 2000: Environmental influences on the rapid intensification of Hurricane Opal (1995) over the Gulf of Mexico. *Mon. Wea. Rev.,* **128,** 322–352.

Braun, S. A., and W.-K. Tao, 2000: Sensitivity of high-resolution simulations of Hurricane Bob (1991) to planetary boundary layer parameterizations. *Mon. Wea. Rev.,* **128,** 3941–3961.

Carr, L. E., III, and R. T. Williams, 1989: Barotropic vortex stability to perturbations from axisymmetry. *J. Atmos. Sci.,* **46,** 3177–3191.

Challa, M., and R. L. Pfeffer, 1990: Formation of Atlantic hurricanes from cloud clusters and depressions. *J. Atmos. Sci.,* **47,** 909–927.

DeMaria, M., 1996: The effect of vertical shear on tropical cyclone intensity change. *J. Atmos. Sci.,* **53,** 2076–2087.

——, and J. Kaplan, 1994a: Sea surface temperature and maximum intensity of Atlantic tropical cyclones. *J. Climate,* **7,** 1324–1334.

——, and J. Kaplan, 1994b: A statistical hurricane intensity prediction scheme (SHIPS) for the Atlantic basin. *Wea. Forecasting,* **9,** 209–220.

——, and J. Kaplan, 1999: An updated statistical hurricane intensity prediction scheme (SHIPS) for the Atlantic and Eastern Pacific Basins. *Wea. Forecasting,* **14,** 326–337.

Eliassen, A., 1952: Slow thermally or frictionally controlled meridional circulation in a circular vortex. *Astrophys. Norv.,* **5,** 19–60.

Emanuel, K. A., 1995: Sensitivity of tropical cyclones to surface exchange coefficients and a revised steady-state model incorporating eye dynamics. *J. Atmos. Sci.,* **52,** 3969–3976.

——, 1998: Theoretical and numerical modeling inferences on the feedback of ocean dynamics on hurricane intensity. Preprints, *Symp. on Tropical Cyclone Intensity Change,* Phoenix, AZ, Amer. Meteor. Soc., 154–159.

——, 1999: Thermodynamic control of hurricane intensity. *Nature,* **401,** 665–669.

——, 2000: A statistical analysis of tropical cyclone intensity. *Mon. Wea. Rev.,* **128,** 1139–1152.

——, M. Fantini, and A. J. Thorpe 1987: Baroclinic instability in an environment of small stability to slantwise moist convection. Part I: Two-dimensional models. *J. Atmos. Sci.,* **44,** 1559–1573.

Frank, W. M., and E. A. Ritchie, 1999: Effect of environmental flow upon tropical cyclone structure. *Mon. Wea. Rev.,* **127,** 2044–2061.

Franklin, J. L., M. L. Black, and K. Valde, 2000: Eyewall wind profiles in hurricanes determined by GPS dropwindsondes. Preprints, *24th Conf. on Hurricanes and Tropical Meteorology,* Fort Lauderdale, FL, Amer. Meteor. Soc., 446–447.

Gray, W. M., 1968: Global view of the origin of tropical disturbances and storms. *Mon. Wea. Rev.,* **96,** 669–700.

Hoskins, B. J., and F. P. Bretherton, 1972: Atmospheric frontogenesis models: Mathematical formulation and solution. *J. Atmos. Sci.,* **29,** 11–37.

Jones, S. C., 1995: The evolution of vortices in vertical shear. Part I: Initially barotropic vorticies. *Quart. J. Roy. Meteor. Soc.,* **121,** 2760–2780.

Krishnamurti, T. N., W. Han, B. Jha, and H. S. Bedi, 1998: Numerical prediction of Hurricane Opal. *Mon. Wea. Rev.,* **126,** 1347–1363.

Kurihara, Y., and R. E. Tuleya, 1974: Structure of a tropical cyclone developed in a three-dimensional numerical simulation model. *J. Atmos. Sci.,* **31,** 893–919.

——, M. A. Bender, and R. J. Ross, 1993: An initialization scheme of hurricane models by vortex specification. *Mon. Wea. Rev.,* **121,** 2030–2045.

——, ——, R. E. Tuleya, and R. J. Ross, 1995: Improvements in the GFDL hurricane prediction system. *Mon. Wea. Rev.,* **123,** 2791–2801.

——, R. E. Tuleya, and M. A. Bender, 1998: The GFDL hurricane prediction system and it performance in the 1995 hurricane season. *Mon. Wea. Rev.,* **126,** 1306–1322.

Liu, Y., D.-L. Zhang, and M. K. Yau, 1997: A multiscale numerical study of Hurricane Andrew (1992). Part I. Explicit simulation and verification. *Mon. Wea. Rev.,* **125,** 3073–3093.

——, ——, and ——, 1999: A multiscale numerical study of Hurricane Andrew (1992). Part II: Kinematics and inner-core structures. *Mon. Wea. Rev.,* **127,** 2597–2616.

Marks, F. D., L. K. Shay, and the Fifth Prospectus Development Team, 1998: Landfalling tropical cyclones: Forecast problems and associated research opportunities. *Bull. Amer. Meteor. Soc.,* **79,** 305–323.

Melander, M. V., J. C. McWilliams, N. J. Zabusky, 1987: Axisymmetrization an vorticity-gradient intensification of an isolated two-dimensional vortex through filamentation. *J. Fluid Mech.* **178,** 137–159.

Möller, J. D., and L. S. Shapiro, 2001: Balanced contributions to the intensification of Hurricane Opal as diagnosed from a GFDL model forecast. *Mon. Wea. Rev.,* submitted.

Molinari, J., and D. Vollaro, 1989: External influences on hurricane intensity. Part I: Outflow layer eddy angular momentum fluxes. *J. Atmos. Sci.,* **46,** 1093–1105.

——, and ——, 1990: External influences on hurricane intensity. Part II: Vertical structure and response of the hurricane vortex. *J. Atmos. Sci.,* **47,** 1902–1918.

——, S. Skubis, D. Vollaro, F. Alsheimer, and H. E. Willoughby, 1998: Potential vorticity analysis of tropical cyclone intensification. *J. Atmos. Sci.,* **55,** 2632–2644.

Montgomery, M. T., and B. Farrell, 1993: Tropical cyclone formation. *J. Atmos. Sci.,* **50,** 285–310.

——, and R. J. Kallenbach, 1997: A theory for vortex Rossby waves and its application to spiral bands and intensity changes in hurricanes. *Quart. J. Roy. Meteor. Soc.,* **123,** 435–465.

——, and J. Enagonio, 1998: Tropical cyclogenesis via convectively forced vortex Rossby waves in a three-dimensional quasigeostrophic model. *J. Atmos. Sci.,* **55,** 3176–3207.

Reasor, P. D., M. T. Montgomery, F. D. Marks, and J. F. Gamache, 2000: Low-wavenumber structure and evolution of the hurricane inner core observed by airborne dual-Doppler rader. *Mon. Wea. Rev.,* **128,** 1653–1680.

Shapiro, L. J., and H. E. Willoughby, 1982: The response of balanced hurricanes to local sources of heat and momentum. *J. Atmos. Sci.,* **39,** 378–394.

Smith, G. B., II, and M. T. Montgomery, 1995: Vortex axisymmetrization and its dependence on azimuthal wavenumber or asymmetric radial structure changes. *Quart. J. Roy. Meteor. Soc.,* **121,** 1615–1650.

Titley, D. W., and R. L. Elsberry, 1999: Rapid intensification of tropical cyclones: A case study of Supertyphoon Flo during TCM-90. Preprints, *23rd Conf. on Hurricanes and Tropical Meteorology,* Vol. II, Dallas, TX, *Amer. Meteor. Soc.,* 588–591.

Willoughby, H. E., 1979: Forced secondary circulations in hurricane. *J. Geophys. Res.,* **84,** 3173–3183.

Wu, C.-C., and H.-J. Cheng, 1999: An observational study of environmental influences on the intensity changes of Typhoons Flo (1990) and Gene (1990). *Mon. Wea. Rev.,* **127,** 3003–3031.

Zhang, D.-L., Y. Liu, and M. K. Yau, 2000: A multiscale numerical study of Hurricane Andrew (1992). Part III: Dynamically induced vertical motion. *Mon. Wea. Rev.,* **128,** 3772–3788.